FRONTIERS OF PHYSICS

RESEARCH ARTICLE
Volume 19 / Issue 2 / 23302 / 2024

Proposal for valleytronic materials: Ferrovalley metal and valley gapless semiconductor

San-Dong Guo[1,†], Yu-Ling Tao[1], Guangzhao Wang[2], Shaobo Chen[3], Dong Huang[1], Yee Sin Ang[4]

1 School of Electronic Engineering, Xi'an University of Posts and Telecommunications, Xi'an 710121, China
2 Key Laboratory of Extraordinary Bond Engineering and Advanced Materials Technology of Chongqing, School of Electronic Information Engineering, Yangtze Normal University, Chongqing 408100, China
3 College of Electronic and Information Engineering, Anshun University, Anshun 561000, China
4 Science, Mathematics and Technology (SMT), Singapore University of Technology and Design (SUTD), 8 Somapah Road, Singapore 487372, Singapore
Corresponding author. E-mail: †sandongyuwang@163.com
Received May 20, 2023; accepted July 26, 2023

ABSTRACT

Valleytronic materials can provide new degrees of freedom to future electronic devices. In this work, the concepts of the ferrovalley metal (FVM) and valley gapless semiconductor (VGS) are proposed, which can be achieved in valleytronic bilayer systems by electric field engineering. In valleytronic bilayer systems, the interaction between out-of-plane ferroelectricity and A-type antiferromagnetism can induce layer-polarized anomalous valley Hall (LP-AVH) effect. The K and –K valleys of FVM are both metallic, and electron and hole carriers simultaneously exist. In the extreme case, the FVM can become VGS by analogizing spin gapless semiconductor (SGS). Moreover, it is proposed that the valley splitting enhancement and valley polarization reversal can be achieved by electric field engineering in valleytronic bilayer systems. Taking the bilayer $RuBr_2$ as an example, our proposal is confirmed by the first-principle calculations. The FVM and VGS can be achieved in bilayer $RuBr_2$ by applying electric field. With appropriate electric field range, increasing electric field can enhance valley splitting, and the valley polarization can be reversed by flipping electric field direction. To effectively tune valley properties by electric field in bilayer systems, the parent monolayer should possess out-of-plane magnetization, and have large valley splitting. Our results shed light on the possible role of electric field in tuning valleytronic bilayer systems, and provide a way to design the ferrovalley-related material by electric field.

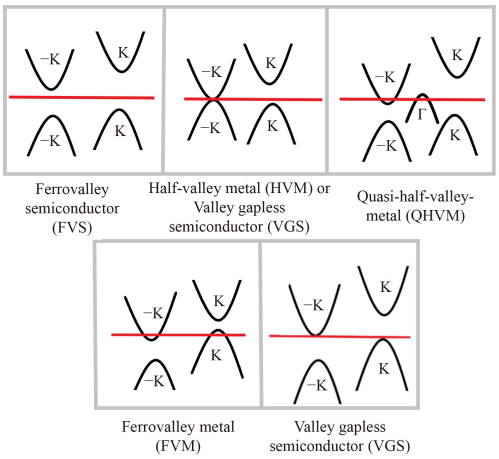

Keywords valleytronics, electric field, bilayer

1 Introduction

Manipulating different degrees of freedom of electrons plays a key role in building modern electronic devices. The valley pseudospin is one of the emerging degrees of freedom beyond charge and spin of carriers [1, 2]. In crystalline solids, valley is characterized by a local energy extreme for both the conduction or valence band. For many MoS_2-like monolayers, their conduction band minimum (CBM) and valence band maximum (VBM)

Higher Education Press

arXiv: 2211.05974
https://doi.org/10.1007/s11467-023-1334-y

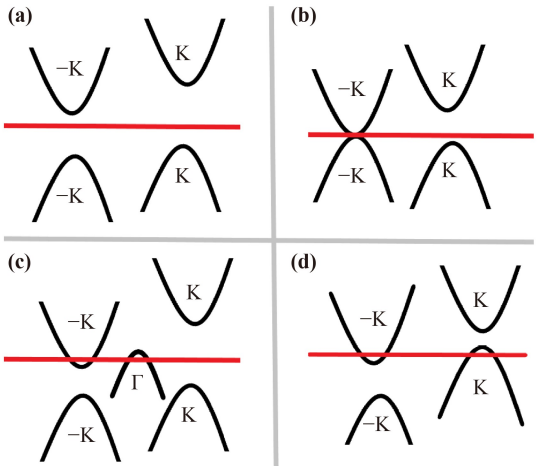

Fig. 1 Schematic diagrams of energy bands of ferrovalley semiconductor **(a)**, half-valley-metal **(b)**, quasi-half-valley-metal **(c)** and ferrovalley metal **(d)**. The horizontal red lines mean Fermi level.

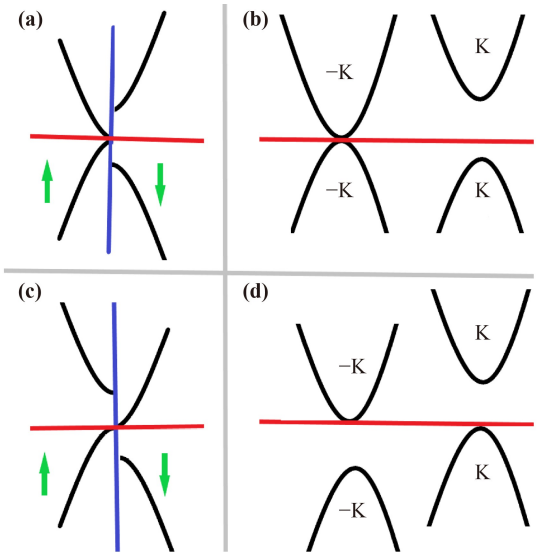

Fig. 2 Schematic diagram of the analogy between spin gapless semiconductor **(a, c)** and valley gapless semiconductor **(b, d)**. The spin-up/spin-down is equivalent to –K/K valley. The green arrows mean spin, and the horizontal red lines mean Fermi level.

are located in two inequivalent momenta –K and K, which constitute a binary valley index [1, 3–9]. The intensive efforts have been made to manipulate the valley pseudospin, and a well-known field is established and called valleytronics [10]. The main challenge for valleytronics lies in inducing valley polarization. For systems with time-reversal symmetry, the optical pumping, magnetic field, magnetic substrates and magnetic doping have been proposed to generate valley-polarized states [3–9, 11, 12]. However, these methods have some disadvantages. The magnetic substrates and magnetic doping destroy intrinsic energy band structures and crystal structures. The optical pumping and magnetic field limit the generation of purely valley-polarized states. The concepts of ferrovalley semiconductor (FVS) [Fig. 1(a)] and half-valley metal (HVM) [Fig. 1(b)] with intrinsic spontaneous valley polarization have been proposed [13, 14], which have been predicted in many two-dimensional (2D) ferromagnets [15–29]. Recently, we have proposed possible electronic state quasi-half-valley-metal (QHVM) [Fig. 1(c)], which contains electron and hole carriers with only a type of carriers being valley polarized [30].

In analogy to ferromagnetic metal in spintronics, we propose the concept of ferrovalley metal (FVM) [Fig. 1(d)], where the K and –K valleys are both metallic. For FVM, electron and hole carriers simultaneously exist, and the Fermi level slightly touches –K and K valleys (CBM and VBM). The concept of the spin gapless semiconductor (SGS) [Figs. 2(a) and (c)], where both electron and hole can be fully spin polarized, has been proposed in spintronics [31]. By analogizing SGS, the concept of the valley gapless semiconductor (VGS), where both electron and hole can be fully valley polarized, is proposed in this work. The schematic diagrams of the analogy between SGS and VGS are plotted in Fig. 2. There are two possible band structure configurations with valley gapless features as illustrated in Figs. 2(b) and (d). For the first case [Fig. 2(b)], one valley is gapless, while the other valley is semiconducting, which is named as VGS-1. In fact, the first case is HVM, which has been proposed in Ref. [14]. In the second case [Fig. 2(d)], there is a gap for both the –K and K valleys, and the Fermi level just touches both K valley in the valence band and –K valley in the conduction band (or –K valley in the valence band and K valley in the conduction band), which is named as VGS-2. The second case is the extreme case of FVM, where the Fermi level exactly touches –K and K valleys (CBM and VBM). The advantages of the VGS over the common FVS are that: (i) no threshold energy is required to excite electrons from occupied states to empty states; (ii) both electron and hole of VGS can be fully valley polarized.

The proposed FVM and VGS can be used to produce valley Hall effect (see Fig. 3). The Berry curvature only occurs around –K and K valleys with opposite signs and unequal magnitudes. Under an in-plane longitudinal electric field E, the nonzero Berry curvature $\Omega(k)$ makes the carriers of –K and K valleys obtain the general group velocity $v_{//}$ and the anomalous transverse velocity $v_{\perp}$ [1]:

$$v = v_{//} + v_{\perp} = \frac{1}{\hbar}\nabla_k \varepsilon(k) - \frac{e}{\hbar} E \times \Omega(k), \quad (1)$$

where $v_{//}$ is along the electric field direction, while $v_{\perp}$ is perpendicular to the electric field and out-of-plane directions. Under an in-plane longitudinal electric field E, for VGS-1, the electron carriers of –K valley turn towards

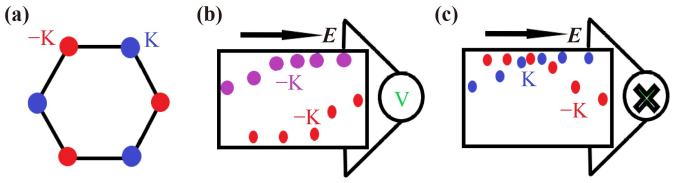

Fig. 3 **(a)** The distribution of Berry curvature, and Berry curvature only occurs around –K and K valleys with opposite signs and unequal magnitudes. Under an in-plane longitudinal electric field E: **(b)** for VGS-1, the electron carriers of –K valley turn towards one edge of the sample, while the hole carriers of –K valley move towards the other edge of the sample, producing measurable valley Hall voltage; **(c)** for FVM and VGS-2, the electron carriers of –K valley and hole carriers of K valley move towards the same edge of the sample, producing non-measurable valley Hall voltage.

one edge of the sample, while the hole carriers of –K valley move towards the other edge of the sample, producing measurable valley Hall voltage. For FVM and VGS-2, the electron carriers of –K valley and hole carriers of K valley move towards the same edge of the sample, producing non-measurable valley Hall voltage.

2 Possible candidates of FVM and VGS-2

It is difficult to find these materials of FVM and VGS-2 in simple compounds. Recently, layer-polarized anomalous Hall effect in valleytronic van der Waals bilayers by interlayer sliding has been proposed, and the parent monolayer should have spontaneous valley polarization [32]. In fact, the pioneering work using sliding ferroelectricity to realize the coexistence of magnetic, ferroelectric and ferrovalley states has been reported in bilayer VS_2 [33]. The interaction between the out-of-plane ferroelectricity and A-type antiferromagnetism allows the realization of layer-polarized anomalous valley Hall (LP-AVH) effect. The ferroelectric switching can induce reversed sign change of valley polarization. The out-of-plane ferroelectricity polarization is equivalent to an electric field [34], so an external electric field can be used to tune layer valley polarization, which provides possibility to achieve FVM and VGS-2. The pioneering work proposing valley manipulation via electric field has been performed in bilayer VSe_2 [35].

As shown in Fig. 4(a), a AB-stacked bilayer lattice, where the parent monolayer has large spontaneous valley polarization in the conduction bands ($d_{x^2-y^2}$+d_{xy}-dominated –K and K valleys of conduction bands), has positive electric polarization, and layer spontaneous valley polarization can be observed [Fig. 4(b)]. Without out-of-plane electric polarization, the energies of –K and K valleys from different layer are coincident. Under the applied electric field, the electrostatic potential of one constituent layer rises and that of the other layer

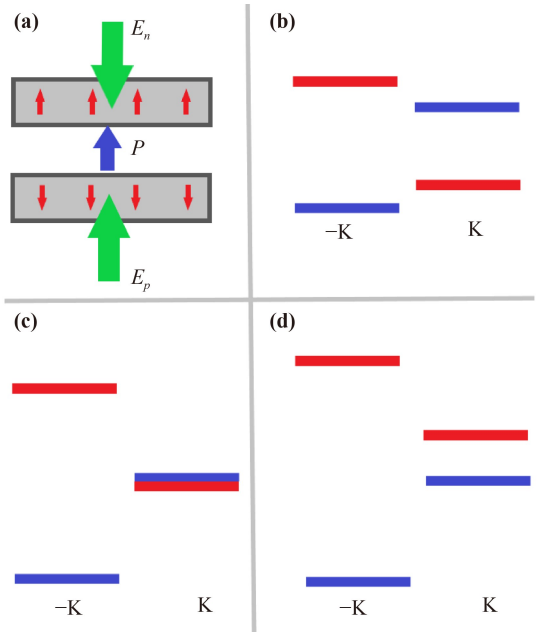

Fig. 4 **(a)** The schematic diagram of a bilayer lattice with AB pattern, and the red, blue and green arrows represents spin, electric polarization P and external electric field E_p (positive z direction) and E_n (negative z direction). The energy level of –K and K valleys without **(b)** and with external electric field $E_p = E_p^c$ **(c)** and $E_p > E_p^c$ **(d)**. The red (blue) energy levels are from up-layer (dn-layer).

decreases, resulting in relative move of energy bands of up and down (dn) layers. By applying an out-of-plane electric polarization or external electric field penetrating from dn-layer to up-layer (defined as the positive field) [see Fig. 4(a)], the energy band from up-layer is shifted toward higher energy with respect to one of dn-layer, which leads to spontaneous valley polarization. As long as the valley splitting of pristine monolayer between –K and K valleys is big enough (The valley splitting of pristine monolaye should be larger than that caused by out-of-plane electric polarization in bilayer system.), the –K and K valleys of bilayer system are from different layer [see Fig. 4(b)]. When increasing positive external electric field E_p, the energy levels at K valley from different layers will coincide at a critical electric field E_p^c [see Fig. 4(c)]. When continuing to increase E_p, the –K and K valleys of bilayer system are from the same dn-layer [see Fig. 4(d)]. When an appropriate positive external electric field ($E_p < E_p^c$) is applied, the spontaneous valley polarization (valley splitting) should be enhanced. However, when the external electric field is reversed (An appropriate negative external electric field (E_n) is applied. This initial negative electric field is used to cancel out-of-plane ferroelectricity polarization field.), the sign of valley polarization can also be reversed (The –K and K valleys along the levels from up-layer and dn-layer exchange each other.). The above analysis also apply to the valence bands (d_{z^2}-dominated –K and K valleys of

valence bands) with small spontaneous valley polarization, and the critical electric field E_p^v is very small. By applying an out-of-plane external electric field penetrating from dn-layer to up-layer, the energy band from up-layer is shifted toward higher energy with respect to one of dn-layer, which can realize FVM and VGS-2.

Here, a concrete example of bilayer $RuBr_2$ is used to illustrate our idea by the first-principles calculations. Calculated results show that increasing electric field indeed can enhance valley splitting in bilayer $RuBr_2$, and make K and –K valleys be from the same layer. The possible electronic states FVM and VGS-2 can be achieved in bilayer $RuBr_2$ caused by electric filed. Our findings can be extended to other valleytronic bilayers, and tune their valley properties by electric field.

3 Computational detail

Within density-functional theory (DFT) [36, 37], the spin-polarized calculations are carried out by employing the projected augmented wave method, as implemented in VASP code [38–40]. We use the generalized gradient approximation of Perdew–Burke–Ernzerhof (PBE-GGA) [41] as exchange-correlation functional. The on-site Coulomb correlation of Ru atoms is considered by the GGA+U method. Based on a linear response approach [42], the self-consistent procedure gives an estimation of $U = 4.99$ eV (see Fig. S1 [43]), which is very larger than $U = 2.5$ eV from comparison with HSE06 result [28]. So, the $U = 2.5$ eV is used within the rotationally invariant approach proposed by Dudarev *et al.* [44]. To attain accurate results, we use the energy cut-off of 500 eV, total energy convergence criterion of 10^{-7} eV and force convergence criteria of 0.001 $\mathrm{eV}\cdot\mathrm{Å}^{-1}$ on each atom. To avoid the interactions between the neighboring slabs, a vacuum space of 20.58 Å is used. The dispersion-corrected DFT-D3 method [45] is adopted to describe the van der Waals interactions between individual layers. The Γ-centered $18 \times 18 \times 1$ k-point meshs in the Brillouin zone (BZ) are used for structure optimization and electronic structures calculations. The spin-orbital coupling (SOC) effect is explicitly included to investigate magnetic anisotropy energy (MAE) and electronic properties of bilayer $RuBr_2$. The Berry curvatures are calculated directly from wave functions based on Fukui's method [46] by using VASPBERRY code [47, 48]. Under an electric field, the atomic positions are relaxed [49].

4 Electronic structures

The LP-AVH effect has been demonstrated in a series of valleytronic materials, such as VSi_2P_4, VSi_2N_4, $FeCl_2$, $RuBr_2$ and VClBr [32]. To clearly demonstrate our previous analysis of electric field effects on valley polarization in valleytronic bilayers (Fig. 4), the parent monolayer should have large valley splitting. The previous works show that $RuBr_2$ has very large valley splitting in the conduction bands or valence bands, which depends on the electronic correlation strength or strain [27, 28]. Therefore, the $RuBr_2$ monolayer is used to validate our proposal.

The $RuBr_2$ monolayer consists Br-Ru-Br sandwich layers, and shares the same crystal structure with MoS_2. It has a hexagonal lattice with the space group $P\bar{6}m2$, and the broken inversion symmetry along with ferromagnetic (FM) ordering can give rise to ferrovalley features. The $RuBr_2$ shows a spontaneous valley splitting of 265 (31) meV in the conduction (valence) band edge at $U = 2.5$ eV [27]. Here, we only construct AB-stacked bilayer of $RuBr_2$, which is plotted in Fig. S2 [43]. The BA-stacked bilayer has the same results with AB-stacked case, when the electric field and sign of valley polarization are simultaneously reversed.

The bilayer $RuBr_2$ has the space group of $P3m1$, whose inversion symmetry and horizontal mirror symmetry are broken. The optimized lattice constant of bilayer $RuBr_2$ is 3.72 Å, and the interlayer distance is 3.16 Å. The AB and BA cases are energetically degenerate with opposite electric polarizations, and connect each other by interlayer sliding [32]. The spontaneous out-of-plane electric polarization is along positive z direction in the AB-stacked bilayer. To determine the ground state of bilayer $RuBr_2$, the intralayer FM and interlayer FM, and intralayer FM and interlayer antiferromagnetic (AFM) magnetic configurations are considered. Calculated results show that bilayer $RuBr_2$ prefers A-type antiferromagnetism with intralayer FM and interlayer AFM orderings. This A-type antiferromagnetism is 7.4 meV per Ru atom lower than that with the FM interlayer exchange interaction.

The energy band structures of AB case are plotted in Fig. 5(a), and the layer-characters and Ru-d-orbital projected energy band structures are also plotted in Figs. 5(b) and (c), respectively. The AB bilayer shows an indirect band gap of 0.373 eV, and the VBM and CBM locate at the K and –K points, respectively. It is clearly seen that the VBM (CBM) is from the up-(dn-)layer (Fig. 5(b) and Fig. S3 [43]), and the valleys are layer-locked with spontaneous valley polarization. The valley splitting in the valence (conduction) bands are defined as: $\Delta E_V = E_V^K - E_V^{-K}$ ($\Delta E_C = E_C^K - E_C^{-K}$), and the calculated value is 4.8 meV (8.10 meV). According to Fig. 5(b), it is found that the valley splitting of conduction band of monolayer $RuBr_2$ is observable, while the valley splitting of valence band is very small, which is due to different distribution of Ru-d orbitals. The valley splitting $|\Delta E|$ can be expressed as [50, 51]: $|\Delta E| = |E^K - E^{-K}| = 4\alpha$ (α is the SOC-related constant), when $d_{x^2-y^2}+d_{xy}$ orbitals dominate the K and –K valleys. If the –K and K valleys are mainly from d_{z^2} orbitals, the valley splitting $|\Delta E|$ will become: $|\Delta E| = |E^K - E^{-K}| \approx 0$.

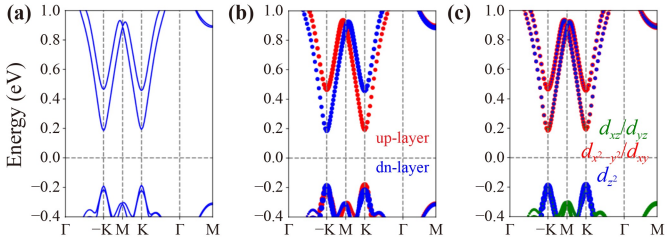

Fig. 5 For AB-stacked bilayer $RuBr_2$, **(a)** the energy band structures; **(b)** layer-characters energy band structures; **(c)** Ru-*d*-orbital projected energy band structures.

Essentially, ferroelectricity polarization and electric field are equivalent to produce valley polarization in valleytronic bilayer. Here, the electric field effects on valley polarization in bilayer $RuBr_2$ are investigated. Firstly, we determine the magnetic ground state under the positive and negative electric field, and the energy differences per Ru atom between interlayer FM and AFM orderings as a function of electric field E are shown in Fig. S4 [43]. Calculated results show that the interlayer AFM state is always ground state within considered E range, and the applied electric field can enhance the interlayer AFM interaction.

The energy band structures of bilayer $RuBr_2$ under representative electric field E are plotted in Fig. 6, and the evolutions of related energy band gap and the valley splitting for both valence and condition bands as a function of E are plotted in Fig. 7. With increasing positive E, the global gap decreases, and a semiconductor to metal transition is induced at $E = 0.30$ V/Å. By applying positive E, the energy band from up-layer is shifted toward higher energy with respect to one of dn-layer. When increasing positive E, the energy levels at K valley from different layers in the conduction bands near Fermi level will coincide at about $E = 0.20$ V/Å. For $E > 0.20$ V/Å, the –K and K valleys of bilayer system in the conduction bands are from the same dn-layer. For the valence bands, these phenomenons can also be observed, and the critical E is very small, which is due to small valley splitting in the valence bands for monolayer $RuBr_2$ at $U = 2.5$ eV. With increasing positive E, the gap of K valley firstly remains almost unchanged, and then decreases. However, for the gap of –K valley, it decreases, and then increases at about $E = 0.35$ V/Å. For 0 V/Å $< E <$ 0.25 V/Å, the valley splitting in the conduction bands increases with increasing positive E. At $E = 0.25$ V/Å, the valley splitting of conduction bands reaches up to 273 meV, which is close to one (265 meV) of monolayer $RuBr_2$ [27]. The analysis above can also be applied to negative E case. The difference mainly includes two aspects: (i) the K and –K valleys exchange each other; (ii) the negative E firstly need to cancel out the small polarized electric field. When an appropriate positive electric field is reversed, the sign of valley polarization can also be reversed.

Figure 8 presents the calculated Berry curvatures $\Omega(k)$ of bilayer $RuBr_2$ under $E = \pm 0.10$ V/Å. The valley splitting for the conduction (valence) band is 130 (30.0) meV at $E = +0.10$ V/Å, and is 104 (30.2) meV at $E = -0.10$ V/Å. These are larger than one of 8.1 meV (4.8 meV)

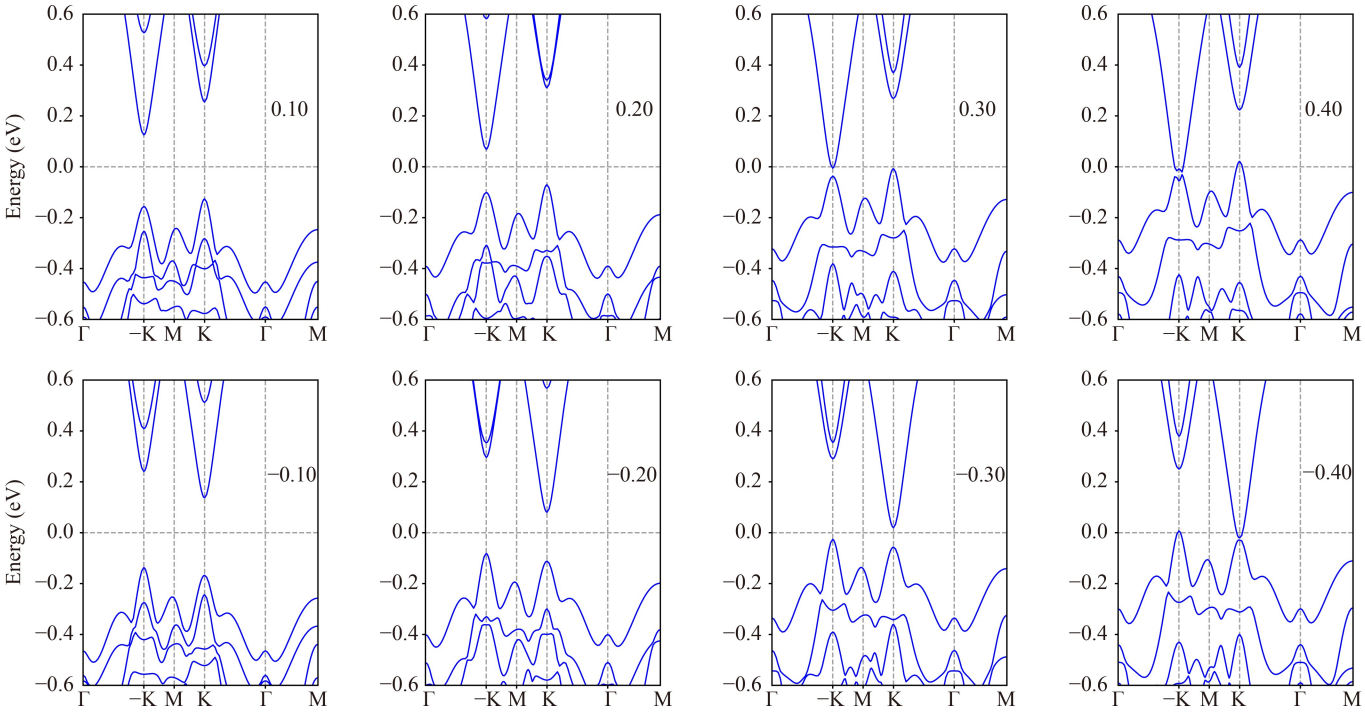

Fig. 6 The energy band structures of AB-stacked bilayer $RuBr_2$ at representative $E = \pm 0.10$, ± 0.20, ± 0.30 and ± 0.40 V/Å.

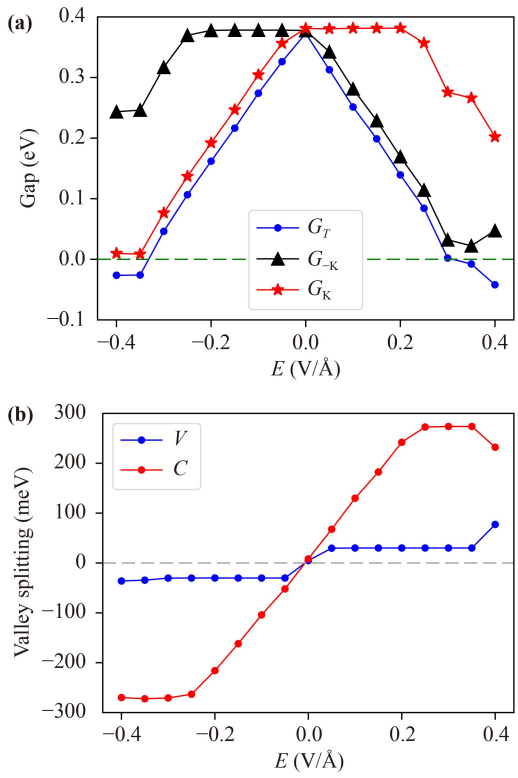

Fig. 7 The related band gaps including the global gap [G_T] and gaps of –K and K valleys [G_{-K} and G_K] **(a)** and valley splitting for both valence [V] and condition [C] bands **(b)** of AB-stacked bilayer $RuBr_2$ as a function of E.

without applying E. For +0.10 V/Å case, the energy of K valley is higher than one of –K valley. The valley polarization can be switched by reversing the electric field direction from $+z$ to $-z$ direction. For the two situations, we observe opposite signs of Berry curvature around –K and K valleys with the unequal magnitudes. By reversing the electric field direction, the magnitudes of Berry curvature at –K and K valleys exchange each other, but their signs remain unchanged. The valley polarization can also be reversed in one-layer FVS with opposite magnetic moment caused by magnetic field, and then the corresponding values of the Berry curvatures at the –K and K valleys will be exchanged [15, 50]. However, the sign of the Berry curvature remains to be the same.

Under an in-plane longitudinal E, Bloch electrons at K and –K valleys will obtain anomalous velocity: $\upsilon \sim E \times \Omega(k)$ [52]. An appropriate doping makes the Fermi level fall between the –K and K valleys. With applied in-plane and out-of-plane electric fields, the Berry curvature forces the carriers to accumulate on one side of one layer of bilayer. When the out-of-plane electric field is reversed, the carriers accumulate on one side of the other layer of bilayer. These give rise to LP-AVH effect.

In the bilayer $RuBr_2$, the FVM can be achieved by

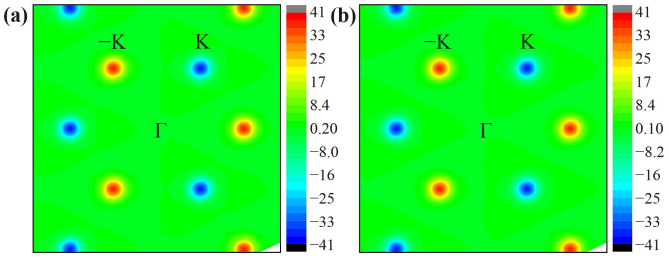

Fig. 8 The Berry curvatures of AB-stacked bilayer $RuBr_2$ in BZ at representative E = +0.10 V/Å **(a)** and –0.10 V/Å **(b)**.

applying electric filed. At E = –0.40 V/Å, the Fermi level slightly touches the K valley of conduction bands and –K valley of valence bands, which can realize FVM. The gaps of –K and K valleys are 244 meV and 10 meV, respectively. At E = +0.40 V/Å, the Fermi level slightly touches the –K valley of conduction bands and K valley of valence bands, and the gaps of –K and K valleys are 47 meV and 202 meV, respectively. However, a band inversion around –K valley can be observed between up and dn layers (see Fig. S5 [43]). In the extreme case, the Fermi level touches the valley bottom of –K valley of conduction bands and the valley top of K valley of valence bands (Fig. 6 at E = +0.30 V/Å), which can achieve VGS-2 [Fig. 2(d)]. Recently, an intense electric field larger than 0.4 V/Å can be produced in 2D materials by dual ionic gating [53], which provides possibility to achieve FVM and VGS-2 in realistic experiments.

5 Discussion and conclusion

For monolayer FVS with hexagonal symmetry, the spontaneous valley polarization depends on the magnetization direction [15–18, 20–28]. For out-of-plane magnetization, the monolayer FVS possess spontaneous valley polarization. However, for in-plane magnetization, no spontaneous valley polarization can be produced. For bilayer system from parent monolayer with in-plane magnetization, the K and –K valleys are from the same layer. By applying an out-of-plane electric polarization or external electric field, the bilayer system has not spontaneous valley polarization. To confirm this, layer-characters energy band structures at E = ±0.15 V/Å are plotted in Fig. S6 [43] with in-plane magnetization. It is clearly seen that the K and –K valleys of both valence and conduction bands are from the same layer, and no spontaneous valley polarization can be observed.

To determine magnetization direction, we calculate the MAE of bilayer $RuBr_2$, which is defined as the energy difference with the magnetization axis along in-plane and out-of-plane directions. The MAE as a function of E is plotted in Fig. S7 [43], which indicates that bilayer $RuBr_2$ favors in-plane magnetization orientation within

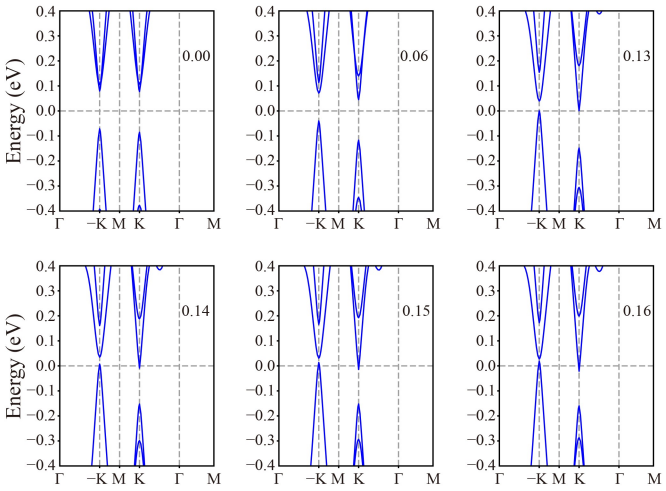

Fig. 9 At $a/a_0 = 0.95$, the energy band structures of AB-stacked bilayer $RuBr_2$ with intrinsic out-of-plane magnetization at representative E.

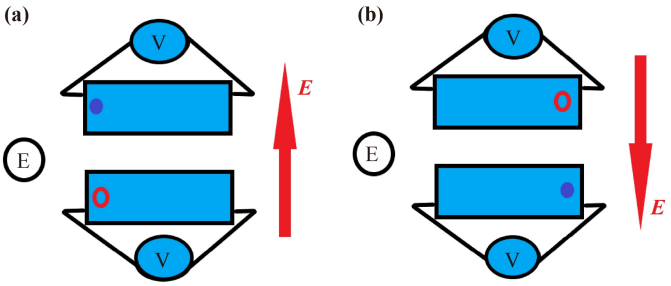

Fig. 10 Under an in-plane longitudinal electric field E (black circles), for bilayer system with suitable out-of-plane electric field (red arrows) producing FVM or VGS-2, **(a)** the electron carriers of one valley and hole carriers of another valley move towards the same edge of the sample in different layer, which should produce measurable valley Hall voltage with opposite sign in different layer; **(b)** when the out-of-plane electric field direction is flipped, the electron carriers of one valley and hole carriers of another valley move towards the opposite edge of the sample in different layer, and the electron and hole carriers will exchange between up and dn layers.

considered E range due to negative MAE. Therefore, bilayer $RuBr_2$ intrinsically has no spontaneous valley polarization at $U = 2.5$ eV. The previous work shows that the magnetic anisotropy direction of monolayer $RuBr_2$ changes from out-of-plane to in-plane one with the critical U value of 2.07 eV [27]. If the real U falls in the range ($U < 2.07$ eV), bilayer $RuBr_2$ will possess spontaneous valley polarization.

Even though the real U falls outside the range, the spontaneous valley polarization can be achieved by strain. By applying strain, the bandwidth can be modified, which effectively controls the relative importance of electronic correlation. To reduce relative importance of electronic correlation, the compressive strain should be used, which equivalently reduces U value. To demonstrate this point, $a/a_0 = 0.95$ biaxial strain is applied on the bilayer $RuBr_2$ with $U = 2.5$ eV. Calculated results show that strained bilayer $RuBr_2$ prefers A-type antiferromagnetism, which is 9.8 meV per Ru atom lower than that with the FM interlayer exchange interaction. The calculated MAE is 909 μeV/Ru, which indicates that strained bilayer $RuBr_2$ favors out-of-plane magnetization orientation. The energy band structures of bilayer $RuBr_2$ is plotted in Fig. S8 [43], and the valley splitting in the valence (conduction) bands is –14.6 meV (–3.0 meV).

To realize FVM and VGS-2, the positive electric filed is applied for AB-stacked bilayer $RuBr_2$ at $a/a_0 = 0.95$ biaxial strain. The energy differences per Ru atom between interlayer FM and AFM orderings as a function of electric field E are shown in Fig. S9 [43], indicating that the interlayer AFM state is always ground state within considered E range. The MAE as a function of E is plotted in Fig. S10 [43], which indicates that bilayer $RuBr_2$ favors out-of-plane magnetization orientation within considered E range due to positive MAE. The total energy band gap as a function of E are plotted in Fig. S11 [43], and the energy band structures with intrinsic out-of-plane magnetization at representative E are plotted in Fig. 9. In the strained bilayer $RuBr_2$, the FVM and VGS-2 can be achieved by applying electric filed. Around $E = 0.15$ V/Å, the Fermi level slightly touches the K valley of conduction bands and –K valley of valence bands, which can realize FVM. In the extreme case, the Fermi level touches the valley bottom of K valley of conduction bands and the valley top of –K valley of valence bands at $E = 0.13$ V/Å, which can achieve VGS-2.

Finally, we discuss how to detect reversed FVM and VGS-2 states in our proposed bilayer system by flipping out-of-plane electric field direction (see Fig. 10). Based on Fig. S5 [43], the VBM and CBM of FVM or VGS-2 state are in different layer. Under an in-plane longitudinal electric field E, the electron carriers of one valley and hole carriers of another valley move towards the same edge of the sample in different layer, which should produce measurable valley Hall voltage with opposite sign in different layer [Fig. 10(a)]. When the out-of-plane electric field direction is flipped, the signs of Berry curvatures of –K and K valleys remain unchanged (see Fig. 8). However, the VBM and CBM exchange between –K and K valleys (see Fig. 6), and the electron and hole carriers will exchange between up and dn layers (see Fig. S6 [43]). And then, the electron carriers of one valley and hole carriers of another valley move towards the opposite edge of the sample in different layer [Fig. 10(b)]. Therefor, the carrier distributions will change by flipping out-of-plane electric field direction.

In summary, we have demonstrated that the electric field can effectively tune valley properties of bilayer $RuBr_2$. The FVM and VGS-2 can be realized in bilayer

$RuBr_2$ by electric field tuning. In addition, the electric field can enhance the valley splitting of bilayer $RuBr_2$, and make the –K and K valleys be from the same layer. We take bilayer $RuBr_2$ as a concrete example, but the analysis can be readily extended to other valleytronic van der Waals bilayers. Our findings can expand understanding of valleytronic van der Waals bilayers, and realize new valleytronic materials: FVM and VGS-2.

Declarations The authors declare that they have no competing interests and there are no conflicts.

Electronic supplementary materials The online version contains supplementary material available at https://doi.org/10.1007/s11467-023-1334-y and https://journal.hep.com.cn/fop/EN/10.1007/s11467-023-1334-y.

Acknowledgements This work was supported by Natural Science Basis Research Plan in Shaanxi Province of China (No. 2020JQ-845). Y.S.A. is supported by the Singapore Ministry of Education Academic Research Fund Tier 2 (Award No. MOE-T2EP50221-0019). We are grateful to Shanxi Supercomputing Center of China, and the calculations were performed on TianHe-2.

References and notes

1. X. Xu, W. Yao, D. Xiao, and T. F. Heinz, Spin and pseudospins in layered transition metal dichalcogenides, *Nat. Phys.* 10(5), 343 (2014)
2. Y. Liu, C. S. Lian, Y. Li, Y. Xu, and W. Duan, Pseudospins and topological effects of phonons in a Kekulé lattice, *Phys. Rev. Lett.* 119(25), 255901 (2017)
3. M. Zeng, Y. Xiao, J. Liu, K. Yang, and L. Fu, Exploring two-dimensional materials toward the next-generation circuits: from monomer design to assembly control, *Chem. Rev.* 118(13), 6236 (2018)
4. K. F. Mak, K. He, J. Shan, and T. F. Heinz, Control of valley polarization in monolayer MoS_2 by optical helicity, *Nat. Nanotechnol.* 7(8), 494 (2012)
5. D. MacNeill, C. Heikes, K. F. Mak, Z. Anderson, A. Kormányos, V. Zólyomi, J. Park, and D. C. Ralph, Breaking of valley degeneracy by magnetic field in monolayer $MoSe_2$, *Phys. Rev. Lett.* 114(3), 037401 (2015)
6. H. Zeng, J. Dai, W. Yao, D. Xiao, and X. Cui, Valley polarization in MoS_2 monolayers by optical pumping, *Nat. Nanotechnol.* 7, 490 (2012)
7. A. Srivastava, M. Sidler, A. V. Allain, D. S. Lembke, A. Kis, and A. Imamoglu, Valley Zeeman effect in elementary optical excitations of monolayer WSe_2, *Nat. Phys.* 11(2), 141 (2015)
8. C. Zhao, T. Norden, P. Zhang, P. Zhao, Y. Cheng, F. Sun, J. P. Parry, P. Taheri, J. Wang, Y. Yang, T. Scrace, K. Kang, S. Yang, G. Miao, R. Sabirianov, G. Kioseoglou, W. Huang, A. Petrou, and H. Zeng, Enhanced valley splitting in monolayer WSe_2 due to magnetic exchange field, *Nat. Nanotechnol.* 12(8), 757 (2017)
9. H. Zeng, J. Dai, W. Yao, D. Xiao, and X. Cui, Valley polarization in MoS_2 monolayers by optical pumping, *Nat. Nanotechnol.* 7(8), 490 (2012)
10. J. R. Schaibley, H. Yu, G. Clark, P. Rivera, J. S. Ross, K. L. Seyler, W. Yao, and X. Xu, Valleytronics in 2D materials, *Nat. Rev. Mater.* 1(11), 16055 (2016)
11. M. S. Mrudul, Á. Jiménez-Galán, M. Ivanov, and G. Dixit, Light-induced valleytronics in pristine graphene, *Optica* 8(3), 422 (2021)
12. M. S. Mrudul and G. Dixit, Controlling valley-polarisation in graphene via tailored light pulses, *J. Phys. At. Mol. Opt. Phys.* 54(22), 224001 (2021)
13. W. Y. Tong, S. J. Gong, X. Wan, and C. G. Duan, Concepts of ferrovalley material and anomalous valley Hall effect, *Nat. Commun.* 7(1), 13612 (2016)
14. H. Hu, W. Y. Tong, Y. H. Shen, X. Wan, and C. G. Duan, Concepts of the half-valley-metal and quantum anomalous valley Hall effect, *npj Comput. Mater.* 6, 129 (2020)
15. S. D. Guo, J. X. Zhu, W. Q. Mu, and B. G. Liu, Possible way to achieve anomalous valley Hall effect by piezoelectric effect in a $GdCl_2$ monolayer, *Phys. Rev. B* 104(22), 224428 (2021)
16. X. Y. Feng, X. L. Xu, Z. L. He, R. Peng, Y. Dai, B. B. Huang, and Y. D. Ma, Valley-related multiple Hall effect in monolayer VSi_2P_4, *Phys. Rev. B* 104(7), 075421 (2021)
17. Q. R. Cui, Y. M. Zhu, J. H. Liang, P. Cui, and H. X. Yang, Spin-valley coupling in a two-dimensional VSi_2N_4 monolayer, *Phys. Rev. B* 103(8), 085421 (2021)
18. X. Zhou, R. Zhang, Z. Zhang, W. Feng, Y. Mokrousov, and Y. Yao, Sign-reversible valley-dependent Berry phase effects in 2D valley-half-semiconductors, *npj Comput. Mater.* 7, 160 (2021)
19. I. Khan, B. Marfoua, and J. Hong, Electric field induced giant valley polarization in two dimensional ferromagnetic $WSe_2/CrSnSe_3$ heterostructure, *npj 2D Mater. Appl.* 5, 10 (2021)
20. H. X. Cheng, J. Zhou, W. Ji, Y. N. Zhang, and Y. P. Feng, Two-dimensional intrinsic ferrovalley GdI_2 with large valley polarization, *Phys. Rev. B* 103(12), 125121 (2021)
21. R. Li, J. W. Jiang, W. B. Mi, and H. L. Bai, Room temperature spontaneous valley polarization in two-dimensional FeClBr monolayer, *Nanoscale* 13(35), 14807 (2021)
22. K. Sheng, Q. Chen, H. K. Yuan, and Z. Y. Wang, Monolayer CeI_2: An intrinsic room-temperature ferrovalley semiconductor, *Phys. Rev. B* 105(7), 075304 (2022)
23. P. Jiang, L. L. Kang, Y. L. Li, X. H. Zheng, Z. Zeng, and S. Sanvito, Prediction of the two-dimensional Janus ferrovalley material LaBrI, *Phys. Rev. B* 104(3), 035430 (2021)
24. R. Peng, Y. Ma, X. Xu, Z. He, B. Huang, and Y. Dai, Intrinsic anomalous valley Hall effect in single-layer Nb_3I_8, *Phys. Rev. B* 102(3), 035412 (2020)
25. K. Sheng, B. K. Zhang, H. K. Yuan, and Z. Y. Wang, Strain-engineered topological phase transitions in ferrovalley 2H–$RuCl_2$ monolayer, *Phys. Rev. B* 105(19), 195312 (2022)

26. S. D. Guo, J. X. Zhu, M. Y. Yin, and B. G. Liu, Substantial electronic correlation effects on the electronic properties in a Janus FeClF monolayer, *Phys. Rev. B* 105(10), 104416 (2022)
27. S. D. Guo, W. Q. Mu, and B. G. Liu, Valley-polarized quantum anomalous Hall insulator in monolayer $RuBr_2$, *2D Mater.* 9, 035011 (2022)
28. H. Huan, Y. Xue, B. Zhao, G. Y. Gao, H. R. Bao, and Z. Q. Yang, Strain-induced half-valley metals and topological phase transitions in MBr_2 monolayers (M = Ru, Os), *Phys. Rev. B* 104(16), 165427 (2021)
29. S. D. Guo, Y. L. Tao, W. Q. Mu, and B. G. Liu, Correlation-driven threefold topological phase transition in monolayer $OsBr_2$, *Front. Phys.* 18(3), 33304 (2023)
30. S. D. Guo, Y. L. Tao, H. T. Guo, Z. Y. Zhao, B. Wang, G. Z. Wang, and X. T. Wang, Possible electronic state quasi-half-valley metal in a VGe_2P_4 monolayer, *Phys. Rev. B* 107(5), 054414 (2023)
31. X. L. Wang, Proposal for a new class of materials: Spin gapless semiconductors, *Phys. Rev. Lett.* 100(15), 156404 (2008)
32. T. Zhang, X. L. Xu, B. B. Huang, Y. Dai, L. Z. Kou, and Y. D. Ma, Layer-polarized anomalous Hall effects in valleytronic van der Waals bilayers, *Mater. Horiz.* 10(2), 483 (2023)
33. X. Liu, A. P. Pyatakov, and W. Ren, Magnetoelectric coupling in multiferroic bilayer VS_2, *Phys. Rev. Lett.* 125(24), 247601 (2020)
34. A. O. Fumega and J. L. Lado, Ferroelectric valley valves with graphene/$MoTe_2$ van der Waals heterostructures, *Nanoscale* 15(5), 2181 (2023)
35. W. Y. Tong and C. G. Duan, Electrical control of the anomalous valley Hall effect in antiferrovalley bilayers, *npj Quantum Mater.* 2, 47 (2017)
36. P. Hohenberg and W. Kohn, Inhomogeneous electron gas, *Phys. Rev.* 136(3B), B864 (1964)
37. W. Kohn and L. J. Sham, Self-consistent equations including exchange and correlation effects, *Phys. Rev.* 140(4A), A1133 (1965)
38. G. Kresse, *Ab initio* molecular dynamics for liquid metals, *J. Non-Cryst. Solids* 193, 222 (1995)
39. G. Kresse and J. Furthmüller, Efficiency of *ab-initio* total energy calculations for metals and semiconductors using a plane-wave basis set, *Comput. Mater. Sci.* 6(1), 15 (1996)
40. G. Kresse and D. Joubert, From ultrasoft pseudopotentials to the projector augmented-wave method, *Phys. Rev. B* 59(3), 1758 (1999)
41. J. P. Perdew, K. Burke, and M. Ernzerhof, Generalized gradient approximation made simple, *Phys. Rev. Lett.* 77(18), 3865 (1996)
42. M. Cococcioni and S. de Gironcoli, Linear response approach to the calculation of the effective interaction parameters in the LDA + U method, *Phys. Rev. B* 71(3), 035105 (2005)
43. See Supplemental Material for calculating U; crystal structures; energy difference between FM and AFM and MAE as a function of E; the related energy band structures.
44. S. L. Dudarev, G. A. Botton, S. Y. Savrasov, C. J. Humphreys, and A. P. Sutton, Electron-energy-loss spectra and the structural stability of nickel oxide: An LSDA+U study, *Phys. Rev. B* 57(3), 1505 (1998)
45. S. Grimme, S. Ehrlich, and L. Goerigk, Effect of the damping function in dispersion corrected density functional theory, *J. Comput. Chem.* 32(7), 1456 (2011)
46. T. Fukui, Y. Hatsugai, and H. Suzuki, Chern numbers in discretized Brillouin zone: Efficient method of computing (spin) Hall conductances, *J. Phys. Soc. Jpn.* 74(6), 1674 (2005)
47. H. J. Kim, URL: github.com/Infant83/VASPBERRY (2018)
48. H. J. Kim, C. Li, J. Feng, J. H. Cho, and Z. Zhang, Competing magnetic orderings and tunable topological states in two-dimensional hexagonal organometallic lattices, *Phys. Rev. B* 93, 041404(R) (2016)
49. To easily meet energy convergence criterion, the parameter DIPOL=0.5 0.5 0.5 is set, and the convergent charge density under small electric field gradually feeds to the calculations with large electric field.
50. P. Zhao, Y. Dai, H. Wang, B. B. Huang, and Y. D. Ma, Intrinsic valley polarization and anomalous valley hall effect in single-layer 2H-$FeCl_2$, *Chem. Phys. Mater.* 1(1), 56 (2022)
51. R. Li, J. W. Jiang, W. B. Mi, and H. L. Bai, Room temperature spontaneous valley polarization in two-dimensional FeClBr monolayer, *Nanoscale* 13(35), 14807 (2021)
52. D. Xiao, M. C. Chang, and Q. Niu, Berry phase effects on electronic properties, *Rev. Mod. Phys.* 82(3), 1959 (2010)
53. B. I. Weintrub, Y. L. Hsieh, S. Kovalchuk, J. N. Kirchhof, K. Greben, and K. I. Bolotin, Generating intense electric fields in 2D materials by dual ionic gating, *Nat. Commun.* 13(1), 6601 (2022)